Investigation of the Novelty Brackets "Gold-S"

F. Pollok, C. von Mandach, S. Griebel, V. Böhm and L. Zentner

Abstract The paper presents the new alternative orthodontic bracket Gold-S. The current applied force of wire on the compliant mechanism and thus its stiffness, will be determined and decreased. Furthermore, the investigation aims on decreasing stiffness by 25 %. Firstly, the geometric CAD model is simulated using the Finite Element Method (FEM), specific parameters are then altered. Accordingly boundary conditions, assumed simplifications and meshing is explained. Secondly, an experimental investigation is conducted, using an additive 3D printing process for the original as well as the improved model. Finally, the occurring forces in both models of the compliant mechanism are displayed in a graph for comparison of simulation and experimental investigation. It turns out that both results are quite similar, even though friction problems were encountered during investigation due to the used model material.

Keywords Compliant mechanisms · Modeling · Brackets · 3D-Printing

F. Pollok (✉) · S. Griebel · L. Zentner
Department of Mechanical Engineering,
Mechanism Technology Group, Technische Universität Ilmenau,
Ilmenau, Germany
e-mail: fabian.pollok@tu-ilmenau.de

S. Griebel
e-mail: stefan.griebel@tu-ilmenau.de

L. Zentner
e-mail: lena.zentner@tu-ilmenau.de

V. Böhm
Department of Mechanical Engineering, Technical Mechanics Group,
Technische Universität Ilmenau, Ilmenau, Germany
e-mail: valter.boehm@tu-ilmenau.de

C. von Mandach
Company Gold-S, Brugg, Switzerland
e-mail: cvmandach@bluewin.ch

L. Zentner et al. (eds.), *Microactuators and Micromechanisms*,
Mechanisms and Machine Science 45, DOI 10.1007/978-3-319-45387-3_18

1 Introduction

Brackets are the most common devices in orthodontics. There are various types and systems, but nowadays only usage of the edgewise bracket has spread throughout the world. An example of a bracket system is shown in Fig. 1. Since its invention in 1925 it maintained its shape and dimensions and consequently its problems. Too strong forces, friction between wire and slot, difficulties with torque control, difficulties with vertical height adjustment and generally with space closure. The reason is:

The high profile causes a lot of functional troubles. Unfortunately, the principle of the invention makes it impossible to reduce the size. There are neither advantages in scaling down the slot nor in reducing the wings. Even self-ligating brackets need additional wings with common dimensions.

Inventor Edward Angle's intention was to reach a precise positioning of the teeth regarding all three planes in space. But already within the first months of development he became aware of the fact, that precise positioning remained complicated. In retrospect several shortcomings of the back then advanced bracket have been revealed. Firstly, the bracket wings in occlusal direction are responsible for both masticatory disturbances and attrition of the upper dentition. They also obstruct tooth movements in the upper jaw. In addition, its design causes a relatively wide gap between wire and tooth surface. Therefore, the wire is required to withstand mastication forces that are many times greater than the forces it has to apply to the teeth. The wire straightens the teeth along its axis mainly in relation to its cross section. The more cross sections of the wire and the slot resemble, the higher are applied forces. The relation is not at all linear, in fact an exponential growth of forces takes place. Hence, wires that correspond to the slot dimensions do not simplify the positioning, but rather complicate it. This seems to be the reason for numerous different and sometimes contradictory treatment techniques, as well as for the amount of contradictory literature on forces, the use of lever arms and moments of force (Burstone 1995; Fiorelli 2016; Hanson 1980; Kesling 2006; Bennett 2014; Antoszewska et al. 2009).

Fig. 1 Bracket from 3 M-Unitek (Unitek 2016)

However, no agreement has been reached regarding the ideal magnitude of forces and moments of force for moving teeth. Good results based on experiences have been published (Burstone 1995; Fiorelli 2016; Hanson 1980; Kesling 2006; Bennett 2014; Antoszewska et al. 2009), but they cover a large range and are usually combined with special treatment methods. Even the highly sophisticated industrial as well as the fully individualised production of brackets do not guarantee a perfect or an easy going treatment. This is because the bracket's slots are only about the same dimension, also the wires have only about the same cross section lengthwise. The faults further increase through bends those are common for precise adjustments. These small invisible deviations will then be 30-fold greater compared to the tooth. So many unpredictable forces exist between wire and slot, varying largely both in direction and range of magnitude. These generate a number of different biological reactions in the periodontium, causing temporally unpredictable side effects and leading to unwanted positions of the teeth. So a considerable part of the effort, made by the precision mechanics industry, crackles without any positive therapeutic influence.

2 Function of the Bracket "Gold-S"

The S-bracket of Gold-S proposes to counter the named disadvantages. The absence of a bonding base and a new wire fixation with a system of different retaining springs (compliant mechanisms) substantially reduce the horizontal contour. The bracket body is no longer milled or casted, but formed by bending a thin foil of metal (cobalt-chrome-alloy), see Fig. 2 for a possible geometry of the base. To produce a functional bracket out of it, several utilities of plastic are part of the invention. An additional protector prevents any soiling of functional areas around the bonding material and a bracket holder (base plate) fixes the tiny spring, which is otherwise difficult to hold within tweezers. Moreover, the bracket holder forms the outer contour of the bonding material and consequently a part of the final bracket body. In addition it fixes a pointer, which is designed to assist the precise positioning of the bracket on the tooth. With this the occlusal contour of the bracket remains a distance less than 1.3 mm away from the tooth surface and the gap

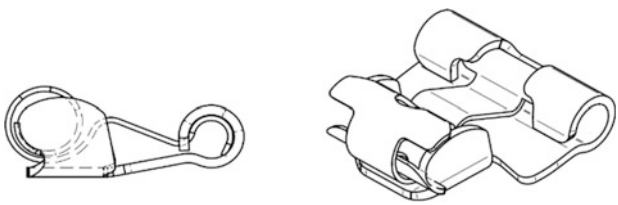

Fig. 2 Side (*left*) and isometric view (*right*) of the bracket system (base plate and compliant mechanism)

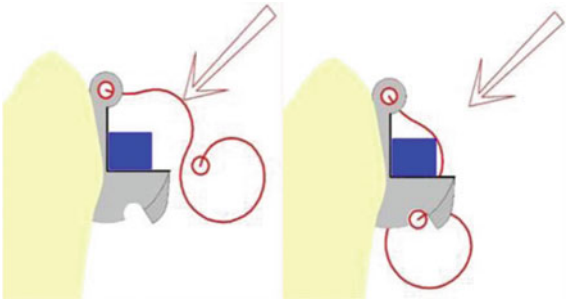

Fig. 3 Open (*left*) and close position (*right*) of the compliant mechanism of Gold-S

between the wire and the tooth surface remains below 0.3 mm. The common slot is replaced by just only a pair of rectangular planes and the fixation of the wire is done by an exchangeable retaining spring, as shown in Fig. 3.

Firstly, the nature of the invention leads even very thin wires within a corresponding small tube, in order to enable the wires great gentle therapeutic potential. Secondly, the spring's elasticity will prevent friction from jamming the wire. Further on it is possible to change the spring, so the rotation of teeth is better controllable. The advantage of a small width lies in an increase of inter-bracket distance and a cubic increase of the wire's elastic range.

This study discusses only the retaining spring with its resilient mechanism and its allotted resilience. A model of this resilient mechanism will be constructed with the finite element method (FEM) to reveal its stiffness. Further on the stiffness will be reduced till the point, where the function as a retaining mechanism ends.

3 Modeling of the Brackets "Gold-S"

Initially, the geometry of the compliant mechanism, given by the patent (VonMandach 2014), is implemented in CAD. The task of this analysis is to identify the applied force of a displaced wire on the compliant mechanism and improve the model, by decreasing its stiffness and hence its force. For this purpose the original version of Gold-S is altered by selected parameters. It aims on decreasing the stiffness of the improved model by 25 % in relation to the original model. This simulation is not a quantitative but a qualitative analysis.

3.1 Geometry and Material of the Brackets "Gold-S"

The flat pattern of the sheet metal with a thickness of 0.08 mm is displayed in Fig. 5. The model is divided into three segments, see Table 1 and corresponding

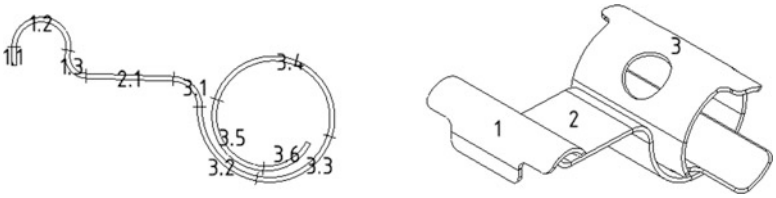

Fig. 4 Sub-segments and ISO-view of the compliant mechanism

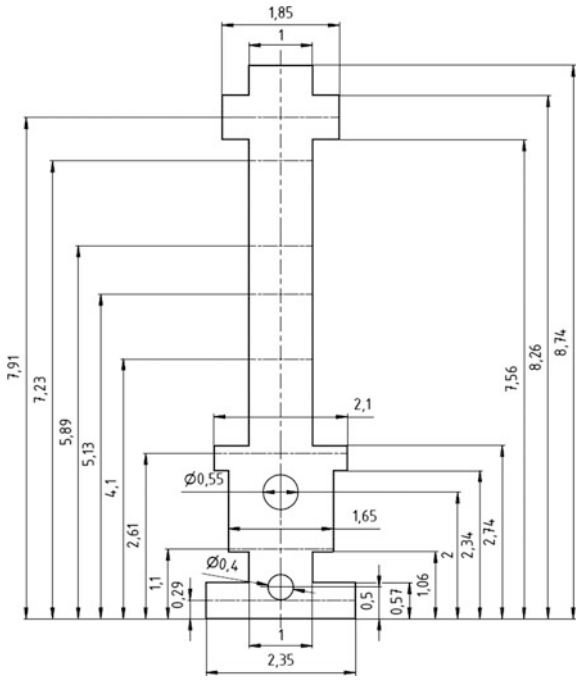

Fig. 5 Dimensions of the flat pattern, bending lines *top* and geometrical edges *bottom* (Pollok 2015)

Fig. 4. Segment 1 is the first support A, Segment 2 is the contact zone between compliant mechanism and wire and Segment 3 is support B. Part 1.2 is the contact surface of the compliant mechanism to the base and allows rotation only. At the subsegment 2.1 is the main contact between the compliant mechanism and the wire. This is the sub-segment through which force is transmitted. Segment 3 is a roll spring with one and a half winding and has the purpose, to compensate the wire's displacement against the compliant mechanism. Its last sub-segment 3.6 is in contact with the base on one edge and can be slightly rotated on this fixed axis (Pollok 2015). For further information see Chap. 3.2.

The wire has a rectangular shape. Its dimensions are 0.4×0.4 mm^2. The used material is a steel laminate of CoCr20Ni16Mo7 and is called "Phynox". The sheet is provided by the enterprise Lamineries MATTHEY SA. The exact material

Table 1 Geometrical parameter for the beam axis of the compliant mechanism (initial geometry)

Parameters	Segment. Sub-segment									
	1.1	*1.2*	*1.3*	*2.1*	*3.1*	*3.2*	*3.3*	*3.4*	*3.5*	*3.6*
Curvature (mm)	–	0.26	0.18	–	0.26	0.73	0.64	0.6	0.53	0.47
Length (mm)	0.2	–	–	0.92	–	–	–	–	–	–
Arc (°)	–	193	100	–	90	80	84	180	104	67
Width (mm)	1	1.85	1	1	1	1	1	2.1	1.65	2.35

chosen is R1500 which has a minimum offset yield point of 1500 N/mm^2. It has an E-module of 210 kN/mm^2 and a Poisson's ratio of 0.3. Phynox is immune to organic acid, relatively resistant to mineral acid and well accepted by the human body. It is a high tech material and commonly used for bio-medical applications (Lamineries MATTHEY SA 2015).

3.2 Groundwork and Boundary Conditions

The Simulation is executed in ANSYS Workbench using geometric nonlinear static structural FEM. The simulation model consists of two bodies, the compliant mechanism and a part of the rectangular wire. As mentioned in Chap. 3 and since the geometry is symmetrical, the model is simplified by dividing both bodies in half. This has to be kept in mind for the analysis, because the resulting force of the simulation needs to be doubled in the end. Also the outer parts in sub-segments 1.2, 3.4 and 3.5 are cut off and reduced to a width of 1 mm.

To keep the meshing process simple, the body is divided into sections. The mesh was initially generated with a finite element size of 0.15 mm. After passing a number of test runs for checking the rightness of the boundary condition and the deformation behaviour, the mesh was refined. The elements of the final refinement have a size of only 0.045 mm. Several comparisons of the averaged and unaveraged stress on surfaces of random samples with a stress gradient reached a difference smaller than 1 %. There are two elements in a row to analyse the stress gradient within the thickness. Used element types are Solid186 and Solid187 with a quadratic approach function (Pollok 2015).

Supports of the model are displayed in Fig. 6. The cut surface is a boundary condition as a *Displacement*, allowing movement in x- and y-direction, but blocking z-movement. The surface of sub-segment 1.2 is a boundary condition as *Remote Displacement* (support A), blocking all movement and rotation except for the rotation around the z-axis in the centre of the radius. The same applies to the support B in sub-segment 3.5, except for this time it is not an area but an edge. The simulation is started by moving the wire 0.35 mm in positive y direction. There are two contact zones. One is between the compliant mechanism 2.1 and the wire, the second one is in segment 3 between the two sides 3.2/3.3 and 3.5/3.6 (Pollok 2015). See Fig. 4 for the selected sub-segments.

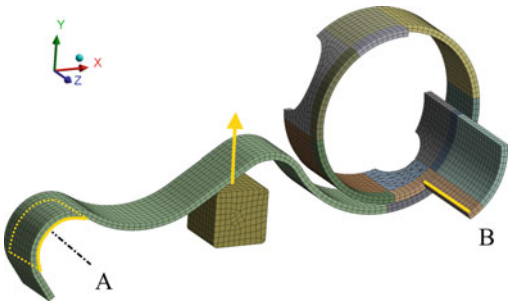

Fig. 6 Supports A and B of the compliant mechanism, allowing rotation around the z-axis. The wire is moved by 0.35 mm along the y-axis (*yellow arrow*). The back of the model, the cut surface, is blocked from moving along the z axis

Table 2 Cases for parameter combination

Cases	h [mm]	b [mm]	r in s-s 1.3 [mm]
I (shape I)	0.05	1	0.18
II	0.05	1	0.73
III	0.05	0.8	0.18
IV (shape II)	0.05	0.8	0.73

3.3 Improvement of Compliant Mechanism Geometry

As monotone behaviour of the model is expected with the given boundary conditions, only the threshold is considered and specific parameters are decreased. The thickness has the most influence on the stiffness of the compliant mechanism. Although the model started with a thickness of 0.08 mm, this is lowered to the final thickness of 0.05 mm before even starting the simulation. Another possible parameter is the width. It is decreased in sub-segments 1.1 to 3.3 from 1 mm to 0.8 mm, so that it still remains in the allowable stress range. Finally the rather hard curvature in sub-segment 1.3 is eased from 0.18 mm to 0.73 mm. The new curvature is tangential to the sub-segments 1.2 and 2.1. The new sub-segment 2.1 can still cover bigger wires than the small used wire (Pollok 2015). Since only the original and the final improved model are interesting for comparison, those are called shape I and shape II. These two shapes are tested on a test setup in Chap. 5. Cases II and III reveal the influence of the adjustments on the model's stiffness. All the parameter changes are listed in Table 2.

4 Results of Modeling

Every alteration on the parameters influenced the stiffness of the simulation model. The enlargement of the curvature had a rather small influence but it is still not negligible. As expected, case IV had the lowest force output of all alternatives. The results of the forces are listed in Table 3. As mentioned in Chap. 3.2, the force has

Table 3 Resulting simulated and actual force

Cases	Nodes/elements	Simulated force [N]	Actual force [N]
I (shape I)	35562/6773	0.791	1.58
II	34323/6510	0.77	1.54
III	31575/5873	0.625	1.25
IV (shape II)	29756/5468	0.598	1.19

to be doubled due to the bisection of the model. A comparison between shape I and II reveals a resulting decrease on stiffness by $\sim$24 %.

5 Experimental Investigations

The experimental investigations will be carried out to verify the modeling results for the compliant mechanism. It should be confirmed experimentally that the stiffness of the new shape II is reduced by about 25 %. Therefore, shape I and shape II are manufactured, measured and compared under the aspect of decreasing stiffness. Because the real dimensions are very small, enlarged demonstrators are investigated experimentally. In order to compare the measurement for these two demonstrators and the simulation model results for both shapes, theoretical considerations should be made first.

Two pairs of systems are considered: (i) shape I and shape II with real dimensions and from material A, (ii) shape I and shape II, which are enlarged in a geometrically similar manner with coefficient k, from material B. The Force F depends on bending stiffness EI_z (E—Young's modulus, I_z—area moment of inertia), the initial curvature κ_0, the length L of the compliant mechanism and the given displacement u_0 of its contact point with the wire (Zentner 2014). To reach the displacement u_0, we require following forces for the first pair (i):

$$F_I = F_I(E_A I_{zI}, L, \kappa_{0I}, u_0), \quad F_{II} = F_{II}(E_A I_{zII}, L, \kappa_{0II}, u_0) \tag{1}$$

The stiffness ratio for pair (i) is F_I/u_0: $F_{II}/u_0 = F_I/F_{II} = \delta$. For the second pair (ii), they are needed forces $F_{k,I}$ and $F_{k,II}$:

$$F_{k,I} = F_{k,I}(E_B k^4 I_{zI}, kL, \frac{\kappa_{0I}}{k}, ku_0), \quad F_{k,II} = F_{k,II}(E_B k^4 I_{zII}, kL, \frac{\kappa_{0II}}{k}, ku_0) \tag{2}$$

The stiffness ratio for this pair (ii) is $F_{k,I}/ku_0$: $F_{k,II}/ku_0 = F_{k,I}/F_{k,II} = \delta k$. According to expressions (1) and (2), ratio δ is equal to ratio δk. Therefore, model results for the shapes I and II and the measurement results for the demonstrators with scale 20:1 can be compared with one another.

5.1 Materials and Methods

For the experimental investigation of the characteristic of the two compliant mechanisms with shape I and shape II, the demonstrators were manufactured in a scale of 20:1.

Due to the complex spatial geometry of the compliant mechanism an additive manufacturing process is chosen. The two mechanisms, the base plate and a stirrup (models the wire) are printed by means of an SLA desktop 3D printer (1 + form, shape Labs Inc., Somerville, United States). In the further course, the stirrup and the base plate are clamped into the pneumatic clamping jaws of a material testing machine. For this reason adhesively-linked supports for clamping are modeled on those. To map the elastic behavior of the compliant mechanisms, a resin (clear resin, shape Labs Inc., Somerville, United States) is used having predominantly brittle and only slightly viscoelastic behavior as a material. In contrast, the stirrup and the base plate made of resin are printed with impact-resistant distinctive properties (tough resin, shape Labs Inc., Somerville, United States) whereby a brittle fracture during the subsequent clamping of the two components can be avoided. All components are printed with a layer thickness of 50 microns. It was ensured that the support structures of the print were at the compliant mechanisms on the front edge side and, in case of stirrup and base plate, at not functionally relevant surfaces. After removal of the support structures, the components are post-cured. Therefor the components are exposed in direct sunlight for several hours. Finally, the components are finished by using emery paper with descending grain size to straighten the end points of the removed support structures and to smoothen irregularities on the contact surfaces of the components to each other.

Figure 7a and b show the two compliant mechanisms of shapes I and II in a top and side view. While shape I has a width of b_I = 20 mm and a radius of curvature

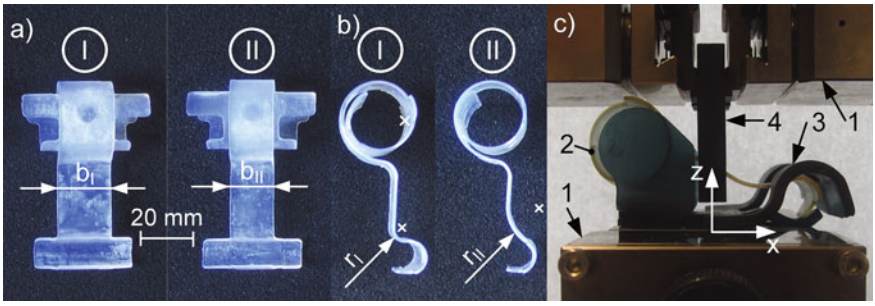

Fig. 7 **a** top and **b** side view of the two, additive manufactured compliant mechanisms with shape I and II at a scale of 20:1; **c** test setup for investigation the compliant mechanism characteristic: (*1*) pneumatic clamping jaws, (*2*) compliant mechanism, (*3*) base plate and (*4*) stirrup

of r_I = 3.6 mm, the improved shape II has a decreased width of b_{II} = 16 mm and a radius of r_{II} = 14.4 mm.

5.2 Experimental Investigation of the Compliant Mechanisms

A materials testing machine (ProLine table testing machine Z005, Zwick GmbH & Co. KG, Ulm, Germany) is used for the metrological examination of the two compliant mechanisms. For this purpose, the base plate is fixed with the bottom pneumatic clamping jaws. Accordingly the assembly of base plate and clamping jaws is immoveable. Then, one of the compliant mechanisms is threaded into the stirrup over an existing slot and the compliant mechanism is spanned on the base plate. After this, the second pneumatic clamping jaw which is fixed on the moveable traverse, is approached to the stirrup so that it can be fixed by the upper clamping jaw. The arrangement of the upper and bottom jaws is rotated by 90° against each other. Hence, the stirrup is perpendicular to the longitudinal axis of the compliant mechanism. Before each trial, the stirrup is moved in z direction until touching the compliant mechanism. Thereby, the zero point is set. A displacement s of 7 mm in positive z-direction is used by moving the stirrup fixed on the traverse. This procedure is done ten times for every compliant mechanism.

The displacement of the traverse is determined with accuracy class 0.5 (according to DIN EN 9513) and a positioning repeatability of the traverse and the associated displacement sensors of ± 2 µm. The corresponding tensile force F in displacement direction is determined by using a 100 N load cell with accuracy class 1 (ISO 7500-1). All measurement values are recorded in the loading phase of the compliant mechanism at a distance of 50 µm and with a 24 bit resolution. The speed of the traverse in this case is set to 15 mm/min. This is a compromise between total test time and influence of viscoelastic material properties on the measured characteristic of the compliant mechanism.

5.3 Results of the Experimental Investigation

Figure 8 (left) shows the raw data of the recorded measurement points of ten test series. It should be noted that taking a global view, the force values of the two compliant mechanisms increase along with the traverse displacement. In addition, the recorded force value F of shape I is higher compared to shape II at the same displacement value of the traverse. Furthermore, a non-continuous rise in the data is determined. Accordingly, the curves have sections with negative slope.

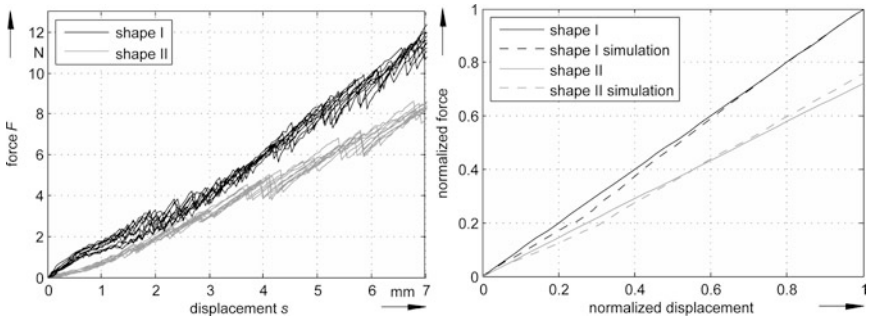

Fig. 8 *Left* Raw data of the n = 10 test series for determination of the compliant mechanism characteristic of shape I (*black line*) and shape II (*grey line*); *right* averaged linear characteristic lines of the compliant mechanisms (shape I and II), average of n = 10 test series, normalized on shape I and compared with the simulation

6 Discussion

The discontinuity of the data from all test series was a result of friction in the real assembly. This is caused by the stick-slip phenomenon whereby the value of sticking friction is significantly greater than the value of sliding friction. Accepting this data, the reason for this may be increased roughness of sliding surfaces (amongst others due to the presence of burrs) as well as a small fit of the components coupling surfaces to each other. Assuming that the compliant mechanism characteristic is linear, each test series was linearized using linear regression in such a way that the resulting straight line extends through the origin. (Hence, the stick-slip phenomenon is no longer visible and the friction is taken into account in the characteristic.) Subsequently, the ten straight lines were averaged for each compliant mechanism and normalized to the final value of the compliant mechanism with shape I, see Fig. 8 (right).

The slope of the straight lines can be equated to the Hooke's law with spring stiffness c. Thus, average spring stiffnesses c_I and c_{II} of 1.587 N/mm and 1.147 N/mm can be calculated for the compliant mechanisms with shape I and II. The ratio between the spring stiffness c_I to c_{II} is $k_E = 0.723$ (k_E – Experiment ratio). Compared with ratio $k_S = 0.757$ (k_S – Simulation ratio) at the end of simulation, a deviation of 4.5 % (0.723/0.757) can be determined.

The deviation is mainly caused by the effects resulting from the manufacturing process. At the anchoring points of support structures, for example, not exactly straight edge line can be achieved. Also, there are manufacture-related variations in thickness and small burrs are present. These are marked in Fig. 9. Through the abrasive finishing procedure of the printed compliant mechanisms, locally material is removed. This also creates deviations from the exact geometry. Further, results from the study of real structures show friction between the components, which was not considered in the simulation.

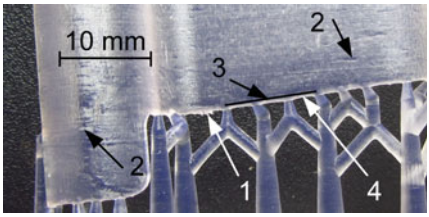

Fig. 9 Detail view of the compliant mechanism with support structures: geometric deviations from exact geometry pointed as (*1*) burr, (*2*) thickness variations, (*3*) and (*4*) not exactly straight running edge course

The simulation results of shape I and II do not have the problem with the stick-slip phenomenon, because of the simplification of the model and other material properties. Therefore there is a bend in the graph visible. This bend is the point of contact between the sub-segments 3.2/3.5 and 3.3/3.6, see Fig. 4. Of course this is not noticeable in the experimental investigation, due to the addressed necessary averaging and linearizing of ten test series.

7 Conclusion and Outlook

As the deviations in both investigations are very small, the requested decrease in stiffness of 25 % could be achieved. The results of the FEM simulations could be verified by the experimental investigations. For further investigations a plurality of compliant mechanisms should be examined to detect manufacture-related variations. Furthermore, measures such as lubrication or subsequent processing of the joining surfaces should be done to minimize the value of sticking friction. Also, measures changing the geometry of the joining surfaces are conceivable (changing the force flow through the joining surfaces). Thus, both can help to avoid stick-slip phenomenon.

References

Antoszewska J, Papadopoulos MA, Park HS, Ludwig B (2009) Five-year experience with orthodontic miniscrew implants: a retrospective investigation of factors influencing success rates. Am J Orthod Dentofacial Orthop 136(2):158.e1–158e10

Bennett JC, McLaughlin RP (2014) Fundamentals of orthodontic treatment mechanics. Hardcover LeGrande Publishing, UK

Burstone CJ, van Steenbergen E, Hanley KJ (1995) Modern edgewise mechanics and the segmented arch technique. Paperback, Ormco Corporation, Horsham

Fiorelli G, Melsen B (2016) Biomechanics in orthodontics, 4th edn. A multimedia interactive textbook. http://www.orthobiomechanics.com/en/

Hanson H (1980) The SPEED system: a report on the development of a new edgewise appliance. Am J Orthod Dentofacial Orthop 78:243–265

Kesling PC (2006) The Tip-Edge PLUS guide and the differential straight-arch technique, 6th edn. Hardcover TP Orthodontics, Westville
Lamineries MATTHEY SA (2015) Phynox, Product Catalogue
Pollok F (2015) Entwicklung eines Feder-Mechanismus für neuartige Brackets (Zahnspange). Bachelor Thesis, TU Ilmenau
Unitek M (2016) Orthodontic Solutions, Product Catalogue; 4.46:88
Von Mandach C (2014) Kit for an orthopedic bracket. Patent specification: WO2015140026 A1
Zentner L (2014) Nachgiebige Mechanismen. De Gruyter Oldenbourg, München